Study on Characteristics of Weld Defect and Its Prevention in Electron Beam Welding (Report II)†
—Some Metallurgical Features of Weld Porosities—

Yoshiaki ARATA*, Kiyoshi TERAI and Shozo MATSUDA****

Abstract

In this report, same as in the previous report, in our attempt to determine the causes of formation of A-porosity, R-porosity and AR-porosity that occur when performing electron-beam welding, we used SUS304 stainless steel and seven kinds of alloys, and we probed weld-metallurgically into the relativity between the porosities, materials and solidifying structure.

A-porosity occurring to stainless steel and carbon steel was recognized mostly along the ripple line, cold shut or bonded part with segregation of manganese being noted on its internal surface. It is presumed that the nitrogen and oxygen contained in the alloys has no direct effect on the occurring of porosity. R-porosity, like A-porosity, was present in abundance along the ripple line with distinct segregation of high vapor pressure elements in the alloys being recognized on its internal surface like manganese in stainless steel and carbon steel and magnesium in 5083 alloy. AR-porosity observable in aluminum alloy saw its incidence mostly along the bonded part and on its internal surface was noted segregation of high vapor pressure element, as in the case of R-porosity.

1. Introduction

Porosity, unmelted lump, cold shut, spiking, etc. are observed as macro weld defects so on except cracks that generally occur in electron beam weld metal.[1] Of these defects, we looked into porosity about its welding condition and its relations with materials and we adopted a slope welding as to the occurring characteristics and reported in our previous report on the result of our finding.

In this report, we found three kinds of porosities, namely, A-porosity, R-porosity and AR-porosity. Occurring of A-porosity is closely concerned with both of the location and shape (length, diameter and profile) of the beam active zone, beam power and its density. R-porosity occurred invariably to all specimens with no direct bearing of the depth of penetration and was closely related to spiking. AR-porosity tended to occur to aluminum and aluminum alloys, and not to be observed in stainless steel and carbon steel.

On the other hand, the longer the nitrogen and oxygen contents in stainless steel and carbon steel, more conspicuous effect there was in evidance on the incidence of A-porosity, R-porosity and their zones increased.

Further, when an element of high vapor pressure like magnesium is contained in pure aluminum, the depth of penetration considerably increases, and also the incidence zone of R-porosity remarkably increases, and its shape looked conspicuously needle-like. In this case, AR-porosity and R-porosity were recognized but no A-porosity did occur.

The porosity diagram which indicated the incidence zones of these porosities by using I_b, $a_b{}^*$ and $\Delta a_b{}^*$ can be utilized for the setting of welding conditions, foreseeing the prevention of their incidence.

The foregoing was an attempt to grasp phenomenally the incidence characteristics of porosities in electron beam welding, but we have not made any metallurgical study of these porosities. Accordingly, we used in this report, same as last time, SUS304 and various other materials in our attempt to determine the causes of formation of A-porosity, R-porosity and AR-porosity that occur in these materials and experimented weld-metallurgically the relativity between the solidification structure and defect incidence.

2. Experimental Procedure

2.1 Material Used

As shown in **Table 1,** seven kinds of alloys were used in this experiment. These materials SUS304 and SUS304N containning 0.2% nitrogen as austenitic stainless steel, semikilled steel SM41 and killed steel S35C as carbon steel, pure aluminum 1200 as aluminum alloy, 5083 containing 4.6% magnesium and 7N01 containing 4.5% zinc and 1.2% magnesium, and we invariably used rolled materials. The specimens we used were 100mm wide, 200—300mm long and 20mm or 30mm thick in shape. Table 1 shows the chemical composition of these materials.

† Received on Dec. 20, 1973
* Professor
** Kawasaki Heavy Industries, Ltd.

Table 1. Chemical compositions of materials used.

Material \ Element	Wt (%) C	Si	Mn	P	S	Fe	Ni	Cr	Cu	Al	Mg	Zn	Others	P.P.m H	O	N
SUS304	0.08	0.79	0.99	0.025	0.010	Bal	8.76	18.29	—	—	—	—	—	4.4	29	230
SUS304N	0.02	0.45	1.53	0.006	0.009	Bal	10.10	18.70	—	—	—	—	—	2.5	99	1950
S35C	0.33	0.25	0.75	0.016	0.017	Bal	—	—	—	—	—	—	—	0.1	6	35
SM41	0.18	0.04	0.79	0.009	0.015	Bal	—	—	—	—	—	—	—	0.0	316	35
1200	—	0.13	0.01	—	—	0.54	—	—	0.03	Bal	—	0.01	—	0.4	24	16
5083	—	0.14	0.64	—	—	0.21	—	0.15	0.04	Bal	4.60	0.01	Ti 0.02	0.4	6	16
7N01	—	0.11	0.39	—	—	0.23	—	0.23	0.07	Bal	1.20	4.64	Ti 0.08 Zr 0.13	0.5	15	8

2.2 Welding Procedure and Welding Condition

Used in the welding was a whole vacuum type electron beam welding machine of Hamilton-type 150 KV-40 mA (6 kW) manufactured by NEC. We conducted a bead on plate test by partial penetration welding with the weld bead placed on the rolled material. As for the procedure, we adopted, same as last time, slope welding, placing the test piece 30° aslant on the table, fixing the electron gun. By moving the table in the oblique angle direction, we had an "upslope" ($\theta_s = +30°$) and "downslope" ($\theta_s = -30°$) weldings.

The welding parameter a_b* adopted here is the ratio between the object distance D_0 and visual focal distance D_F*, and it is called a visual beam active parameter. We conducted slope welding in such a manner as to provide a range of a_b*$=0.46\sim0.93$ at D_F* $=280$mm by changing D_0 against a constant welding condition. The welding condition adopted was the one that selected a condition typical of causing porosity in the test reported last time, and **Table 2** shows these conditions.

Table 2. Welding conditions used in this experiment.

Materials \ Welding conditions	Beam voltage Vb (KV)	Beam current Ib (mA)	Welding speed Vb (cpm)	Visual focal length D_F(mm)	Slope angle θs (°)	Pressure Pch(Torr)
SUS 304	150	30	30	280	±30	4×10^{-4}
SUS 304N	〃	〃	60	〃	〃	〃
S35C	〃	〃	60	〃	〃	〃
SM41	〃	〃	30	〃	〃	〃
1200	〃	〃	60	〃	〃	〃
5083	〃	〃	〃	〃	〃	〃
7N01	〃	〃	〃	〃	〃	〃

To indicate the shape of penetration in the cross section of the welding bead, we used an effective penetrometer $\tilde{P}_p \equiv h_p/\tilde{d}_B$, where h_p meaning depth of penetration, and $\tilde{d}_B$ the effective bead width.[2]

2.3 How to Observe Porosity

As for the porosities existing in the welded parts by partial penetration in the bead on plate test of these test pieces, we confirmed discrimination and its scope by the X-ray permeation test.

Furthermore, in the longitudinal section and cross section of the bead we conducted observation of the depth of penetration, inner surface of the porosities and the solidification structure around them as well as the analysis of the composite elements by optical microscope, scanning electron micrographs and EPMA.

We also checked the precence of gas in the interiors of porosity by manufacturing on experimental basis a simple gas detecting device. **Fig. 1** shows the sketch of this device, actual view of the experiment and the shape of the test piece.

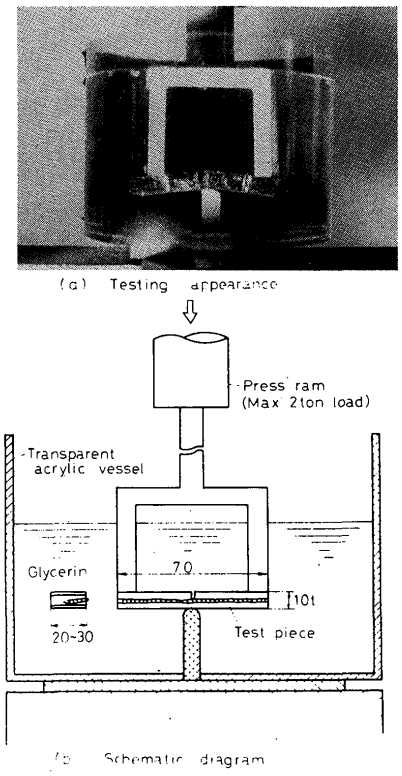

Fig. 1. Side bending test method of weld bead.

3. Results of Experiment

3.1 Occurring appearance of porosities and its micro structure

Photo. 1 and **2** are radiographs taken from side of the part welded on a constant welding condition shown in Table 2 about each materials. **Photo. 3** and **4** show the longitudinal section macroscopic structure of the typical weld metal and the microscopic structure of the cross section of the neighborhood of the porosity.

a) Austenitic Stainless Steel

R- porosity observable in the SUS304 welds indicates that a_b* occurs to the root section over a wide range of 0.50～0.90 and its occurring location is recognized mainly at the top of strong spiking as is observable in the macroscopic structure. A-porosity occurs most abundantly in the 0.70～0.80 range of a_b*, or in the neighborhood of the just focus position of the equivalent beam. It is evident that this tendency is more remarkable in the upslope rather than in the downslope welds.

The R-porosity occurring to SUS304N with large nitrogen content indicates the same tendency as SUS304, but its occurring number and size far exceeds those of SUS304. A-porosity occurs in the range of 0.60～0.85 of a_b*, and, as compared with SUS304, it far exceeds the latter in range, occurring

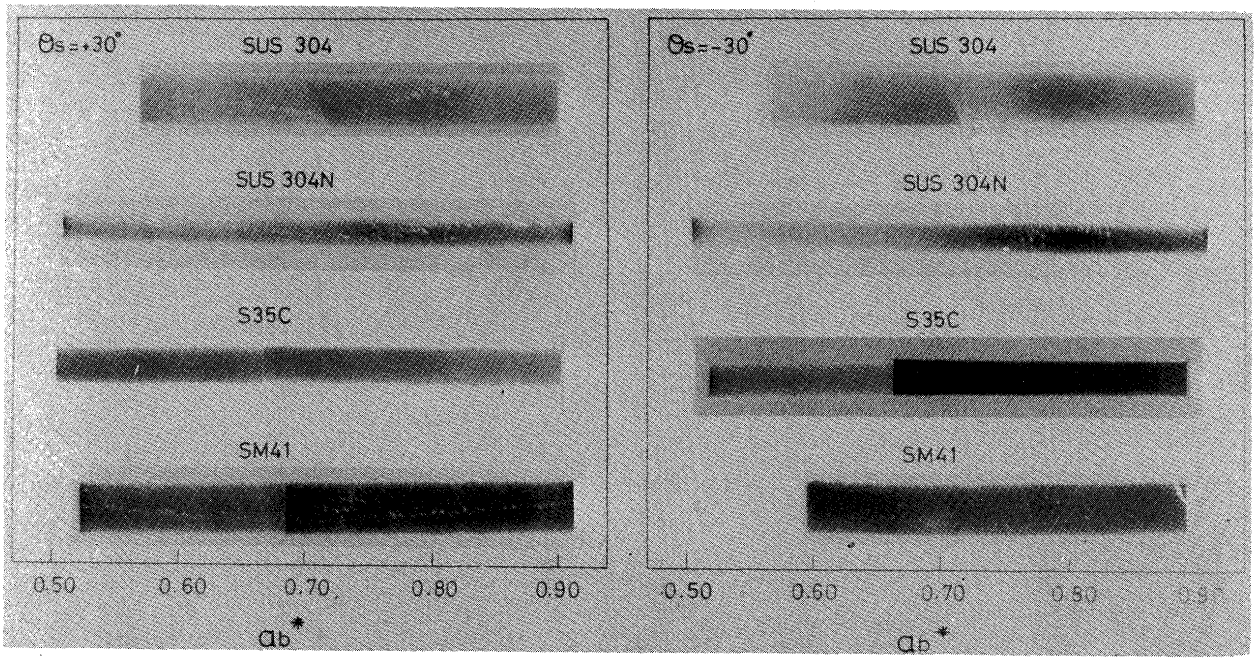

Photo. 1. Radiographs of electron beam welds in iron-based alloy.

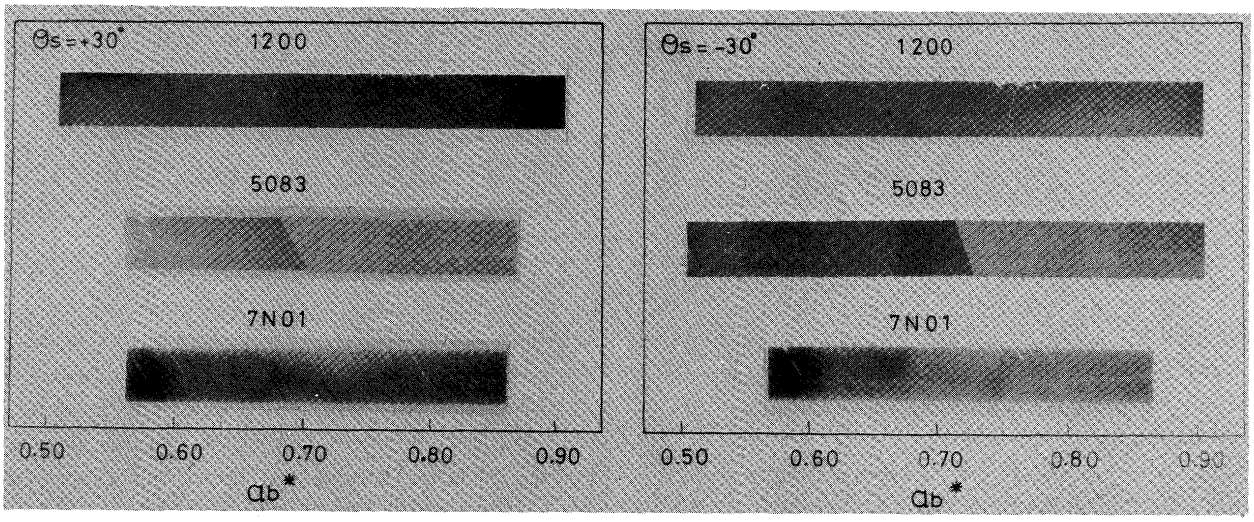

Photo. 2. Radiographs of electron beam welds in aluminum based alloy.

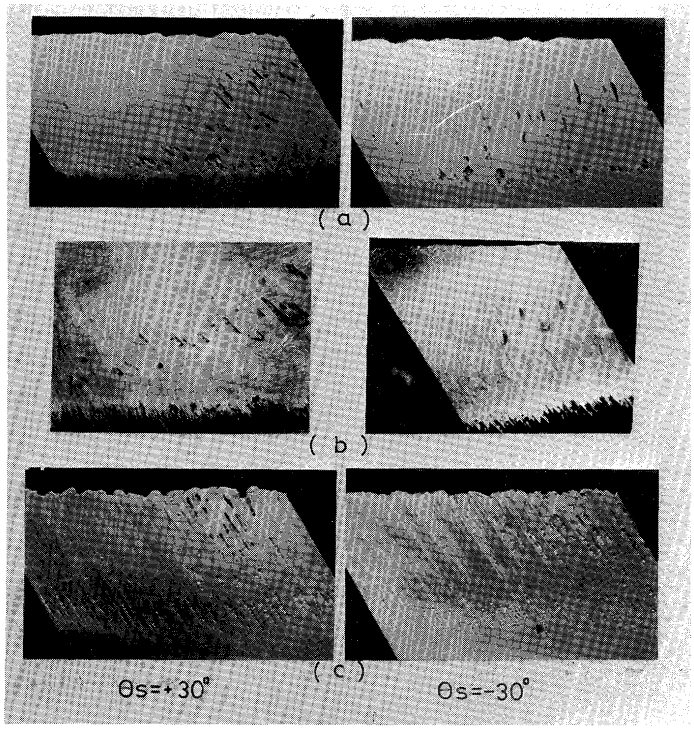

Photo. 3. Longitudinal section macroscopic structure showing typical porosities occurring to the electron beam welds (near to focal point)
(a) SM41 (b) SUS304 (c) 7NO1

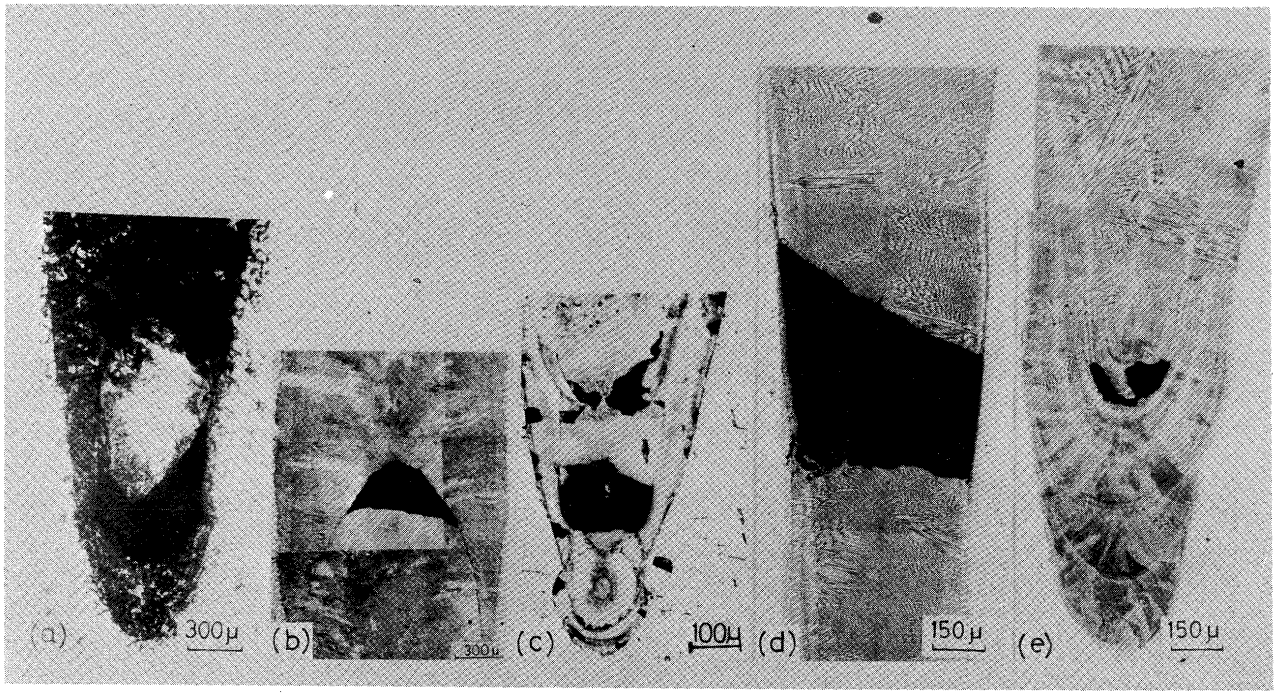

Photo. 4. Microscopic structure near the porosities occurring to weld metals in iron-based alloy.
(a) SM41, R-porosity (b) SUS304, A-porosity (c) SUS304, R-porosity (d) SUS304N, A-porosity (e) SUS304N, R-porosity

number and size. This tendency was more prominent in the upslope rather than in the downslope welds. It seems that this can be attributed to the behavior of nitrogen contained in the alloy.

Photo. 4 b～e show cross section microscopic structure in the neighborhood of the typical R-porosity and A-porosity occurring to the welds of SUS304 and SUS304N. As is seen in this structure, R-porosity occurs to the vicinity to the spikes at the top of the root part with both alloys. The tendency is more common along the ripple line or cold shut, and in evidence is a phase which appears to have been due to the insufficient inflow of molten metal accompanied with rapid solidification in the welding

process.

A-porosity differs slightly in the tendency of occurring between SUS304 and SUS304N. In SUS304, shape of knobby penetration is present in the neighborhood which is considered to correspond to the focus position of the equivalent beam the porosity were mostly along the ripple line in the upper part of the knob. In SUS304N, A-porosity occurs in most cases along the bonded part with no possible linking with ripple line.

In any way, it is considered that the occurring of porosity links with the evaporation element or internal pressure by gas composition and capillary equilibrium accompanying rapid solidification.

b) Carbon Steel

In the upslope welding in S35C, the occurring of R-porosity is in the range of 0.70～0.80 of a_b^* and 0.55～0.60 in the downslope welding and it has more effect with spikes rather than with the depth of penetration. On the other hand, A-porosity slightly occurs, whereas in SM41, R-porosity occurs over the wide entire range of 0.46～0.93 test conditions of a_b^* as compared with S35C. As for A-porosity also, it is quitely conspicuous in the 0.70～0.80 range of a_b^*, which indicates that oxygen content in the alloys is largely responsible for that.

The R-porosity and A-porosity that occur to the welds of S35C and SM41 are occurred mostly along the ripple line or cold shut as in the case of SUS304.

c) Aluminum Alloy

The R-porosity that occurs to pure aluminum 1200 is recognized in the 0.55～0.85 range of a_b^*, the occurring tendency is more frequent in the upslope welds than in the downslope welds. The occurring appearance is connected with the spiking at the top of the root part, and is needle-like as compared with iron based alloys. A-porosity and AR-porosity occurs to the vicinity of 0.70～0.80 just focus of a_b^*, and the number of occurring is far smaller as compared with other aluminum alloys. The depth of penetration had a tendency of being shallow as compared with 5083 and 7N01.

In 5083, R-porosity was present over the entire test area of 0.46～0.93 of a_b^* in both the upslope and downslope welding parts, with strong spikes in abundance as compared with 1200. Accordingly, the porosity showed a shape of much longer needle. AR-porosity occurred to the 0.70～0.80 range of a_b^*, connected with bead surface to be in accord with the radiation direction of the beam.

This tendency was more conspicuous in 7N01 than in 5083. The incidence of AR-porosity was more prominent in the vicinity of focus where the energy intensity is considered to be highest. This indicates that it has a strong effect on the incidence of porosity of alloy element of high vapor pressure.

Photo. 5 shows the microscopic structure around these porosities. R-porosity in most cases present

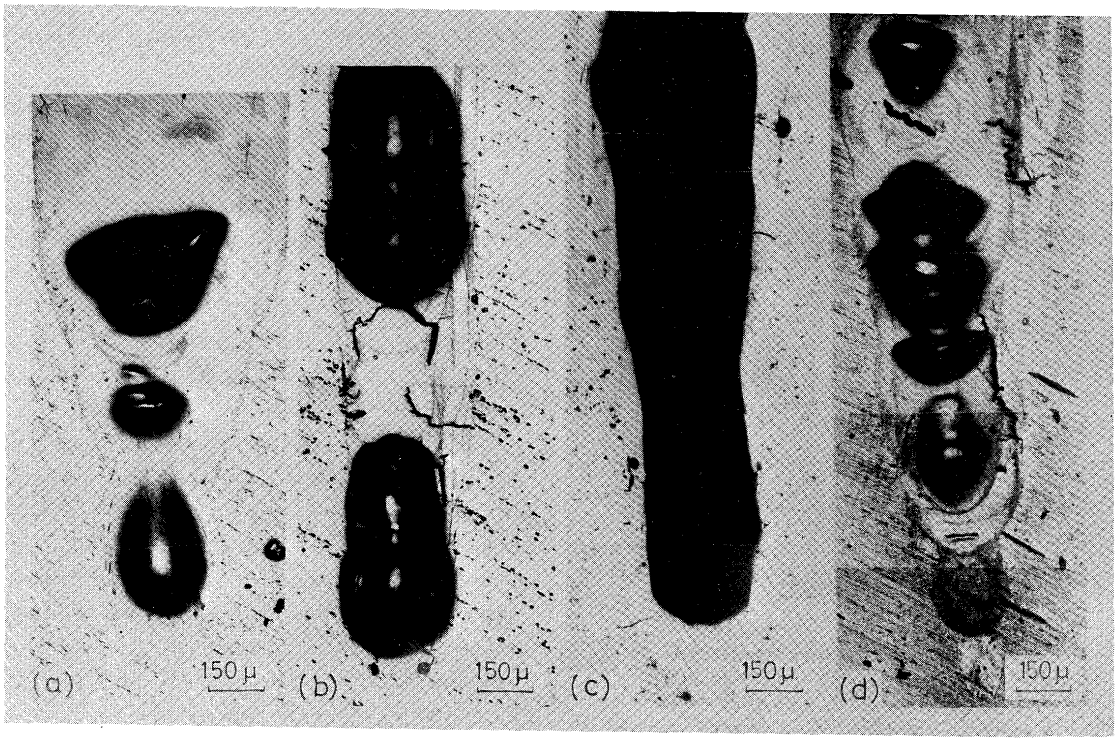

Photo. 5. Microscopic structure near the porosities occurring to weld metals in aluminum-based alloy.
(a) 1200, R-porosity (b) 5083, R-porosity (c) 7N01, AR-porosity (d) 7N01, R-porosity

intermittently along the ripple line or bonded parts, while AR-porosity were observed mostly along the bonded parts in all alloys.

3.2 Observation of the Internal Surface of Porosity and Result of Composition Analysis

Photo. 6 and **7** show scanning electron micrographs of the internal surface of the typical porosities that occur to the welded parts of SUS304 and six other specimens.

The internal surfaces of the porosity observable at the welded parts of SUS304 and SUS304N presented cellular structure, and the size of cells was nearly equal to that of the solidification structure in the central part of the deposit metal, and A-porosity had larger cells than R-porosity. On the internal surface of A-porosity was observed a comparatively small spatter in the input direction of the beam, but it was scarcely seen in R-porosity.

The internal surfaces of the porosities of S35C and SM41 also presented cellular structure similar to those of SUS304 and SUS304N.

Generally, in the solidification structure of the solid-liquid interface by Decant method, it is known

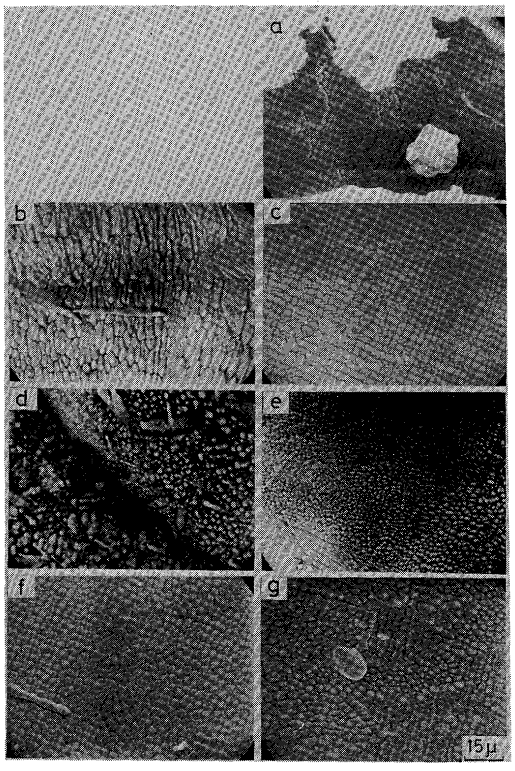

Photo. 6. Scanning electron micrographs of the internal surface of the porosities occurring to weld metals in iron-based alloy.
(a) S35C, R-porosity (b) SM41, A-porosity
(c) SM41, R-porosity (d) SUS304, A-porosity
(e) SUS304, R-porosity (f) SUS304N, A-porosity
(g) SUS304N, R-porosity

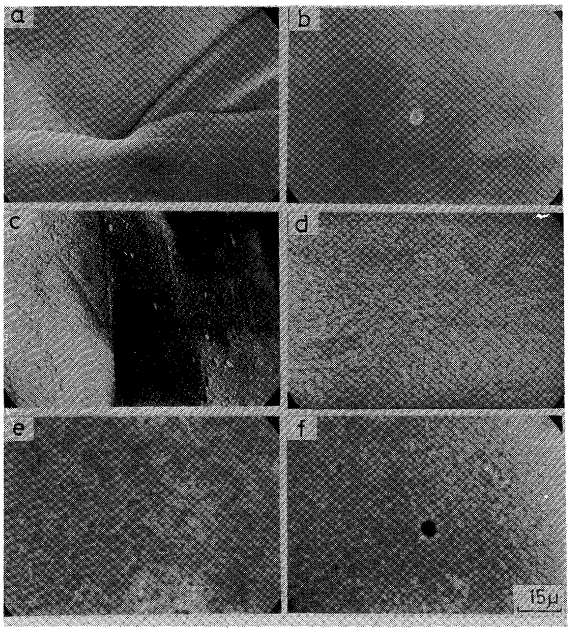

Photo. 7. Scanning electron micrographs of the internal surface of the porosities occurring to weld metals in aluminum and its alloy.
(a) 1200, AR-porosity (b) 1200, R-porosity
(c) 5083, AR-porosity (d) 5083, R-porosity
(e) 7NO1, AR-porosity (f) 7NO1, R-porosity

that, when temperature gradient becomes exceedingly sharp as compared with the growing speed of crystalization, its interface presents cells or cellular structure.[3)]

The internal surface of the porosity of 1200 visually presents metallic lustre, and the pattern of the internal surface differs slightly from other alloys, showing fairly large crystal grains whose size is larger in AR-porosity than in R-porosity. Although ripple pattern is observed in abundance in AR-porosity, it is non-existent in R-porosity.

The internal surface of 5083 porosity looks white (confirmed to be Mg by EPMA) with what appears visually to be deposits of metallic vapor that came into being by the beam radiation or boiling, and its internal surface mostly has a pattern of pockmarks or cellular structure.

On the other hand, 7N01 also, like 5083, in all its porosity internal surfaces looks like zinc-like silver white and its internal surface mostly has a pattern of fine cellular network.

Table 3 shows the results of the spot analysis test by EPMA made on the internal surfaces of these porosities. However, no quantitative correction like absorption effect, fluorescent enhancement by spectrum, etc. has been made about their measured values. The values in the table are indicated in terms of strength ratio between the deposit metal in the neighborhood of each porosity and the internal surfaces of the respective porosities.

From these results abnormal segregations of about 5～13 times (or approximately 4～9%) of manganese

Table 3. Result of EPMA on the internal surface of porosities of various specimens.

Materials and porosity \ Elements			C	Si	Mn	Fe	Ni	Cr	Al	Mg	Zn	O	N
Iron base alloy	S35C	R-porosity	—	—	8.90	—	—	—	—	—	—	—	—
	SM41	A-porosity	1.00	—	5.80	0.95	—	—	—	—	—	—	—
		R-porosity	1.03	—	12.80	0.89	—	—	—	—	—	—	—
	SUS304	A-porosity	0.98	1.00	4.50	0.91	0.77	1.01	—	—	—	—	(1.00)
		R-porosity	—	1.30	5.60	0.93	1.00	1.03	—	—	—	—	(1.00)
	SUS 304N	A-porosity	—	2.90	10.50	0.83	0.61	1.12	—	—	—	—	(0.97)
		R-porosity	—	1.72	3.43	—	0.87	1.01	—	—	—	—	—
Aluminum and aluminum alloy	1200	AR-porosity	—	—	1.01	1.21	—	—	0.99	—	—	—	—
		R-porosity	—	—	0.98	1.12	—	—	1.00	—	—	—	—
	5083	AR-porosity	—	—	0.85	0.58	—	—	0.60	6.50	—	—	—
		R-porosity	—	—	0.85	0.54	—	—	0.79	3.30	—	—	—
	7N01	AR-porosity	—	—	1.15	1.11	—	—	0.55	2.50	9.60	—	—
		R-porosity	—	—	1.00	1.00	—	—	—	1.10	3.96	—	—

Intensity ratio (Intensity of the deposite metal=1.00)

in both the carbon steel and stainless steel are recognized. It was further recognized that the segregation of other elements was only slight.

In the internal surface of 1200 porosity slight segregation of iron contained as impurity was recognized, but segregation was simply negligible. Abnormal segregation was recognized to the tune of 3–6 times (approximately 14–30%) of magnesium in 5083, about 10 times (approximately 45%) of zinc in 7NO1 and 2.5 times (approximately 3%) of magnesium as well.

These elements, which are elements of high vapor pressure, of the composition elements in the alloys, and they are selectively segregated.

3.3 Result of Analysis of Composition Elements of Weld Metal

Shown in **Tables 4, 5** and **Fig. 2** are the analytic results of the composition elements of the weld metal on a constant welding condition with a_b* as parameter about SUS304 and 5083, and their relationship with the effective penetroparameter $\tilde{P}_p$.

According to the said result, in SUS304, the smaller the $\tilde{P}_p$ value (the larger the effective bead width $\tilde{d}_B$) the larger will grow the decrease of composition element, particularly manganese but the decrease of manganese was scarcely noticeable above

Table 4. Result of chemical analysis of weld metals in SUS304.

$\tilde{P}_P$ parameter	a_b*	C	Mn	S	Ni	Cr
0.2	2.0	0.06	1.17	0.008	8.77	18.19
1.1	1.2	0.07	1.24	0.008	8.69	18.32
2.5	1.0	0.07	1.33	0.009	8.77	18.42
4.9	0.75	0.06	1.41	0.008	8.70	18.26
17.8	0.75	0.07	1.65	0.008	8.66	18.41
Base metal		0.08	1.64	0.010	8.70	18.43

Table 5. Result of chemical analysis of weld metals in 5083 alloy.

$\tilde{P}_P$ parameter	a_b*	Fe	Mn	Mg	Cu
0.4	2.0	0.28	0.58	2.94	0.04
2.3	1.2	0.27	0.56	3.91	0.06
6.3	1.0	0.25	0.56	4.25	0.04
8.9	0.75	0.26	0.56	4.48	0.04
>21.4	0.75	0.28	0.56	4.62	0.03
Base metal		0.25	0.57	4.58	0.04

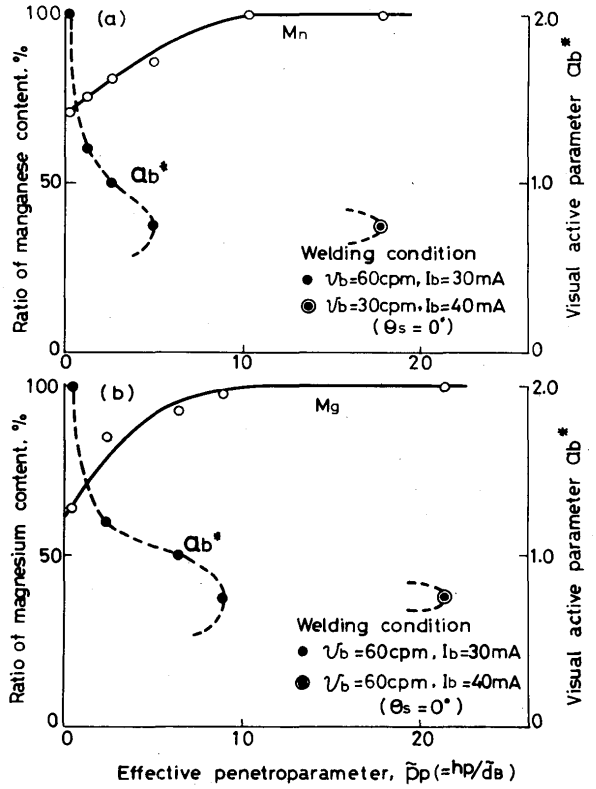

Fig. 2. Relations between a_b*, $\tilde{P}_p$ value and element in the weld metals.
(a) SUS304 (b) 5083

$\widetilde{P}_p \fallingdotseq 10$. In other words, the higher the energy density of the beam and the closer the shape grows to that of deep penetration, the evaporation of the composition element, especially the element of high vapor pressure, becomes less.

This tendency is the same with the behaviors of Mg in 5083 alloy, while no change to speak of took place in other alloy elements. The gas content in the weld metal of SM41 and SUS304N containing oxygen and nitrogen in abundance, as a result of analysis, disclosed nearly equal values with O_2 and N_2 contained in the base metal.

Also as a result of study of the presence of gas in the porosity by simple gas detection device, both SM41 and SUS304N had gas-free porosities. From the foregoing it is considered that oxygen and nitrogen had no direct connection with the incidence of porosities, but they seem to have something to do with the vapor pressure and fluidity of the molten metal containing oxygen and nitrogen in abundance in the melting and solidification process.

3.4 Macroscopic Structure of the Section near Drilled Part

By observing the condition of the bead section of the object to be welded that instantly stopped the beam incidence in the course of the electron beam welding, we watched the behavior of its fluidity. **Photo. 8** and **9** show its result.

As a result, it was discovered that the drilled parts of S35C and SUS304 are almost wholly filled with molten metal, showing comparatively good fluidity, while the drilled parts of SM41 and SUS304N with large contents of oxygen and nitrogen have scanty filling of molten metal and this tendency was more prominent in the upslope welding than in the downslope welding.

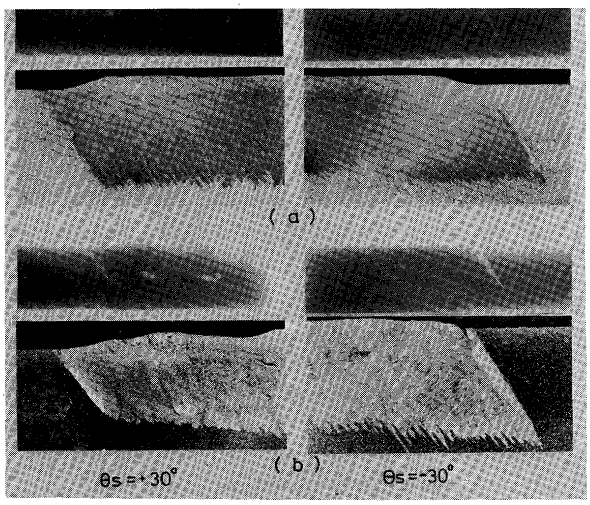

Photo. 8. Radiographs and macroscopic structure near the capillary in austenitic stainless steel.
(a) SUS304 (b) SUS304N

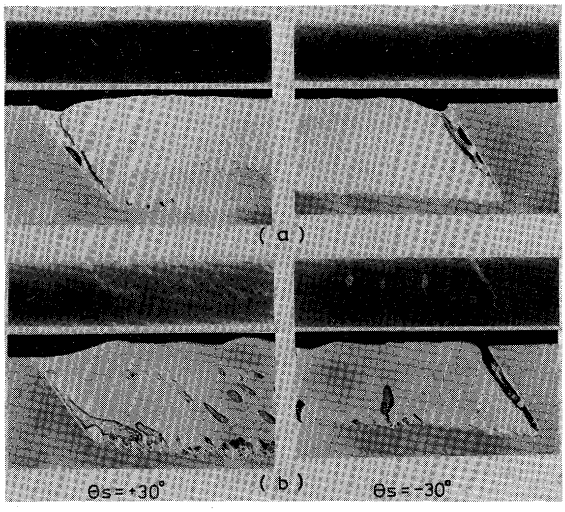

Photo. 9. Radiographs and macroscopic structure near the capillary in carbon steel.
(a) S35C (b) SM41

4. Consideration about Porosity Incidence

From the result of the above experiment, we considered the possible causes of incidence of A-porosity, R-porosity and AR-porosity. Generally, heat source of extremely high energy density is used in the electron beam welding so much so that when electron beam is radiated to the object to be welded violent vaporization by melting and boiling instantly takes place to speak drilling, making possible welding of deep penetration.

The hole thus formed is filled with molten metal in the vicinity of the surface and the molten metal is pushed up again by the vaporization element and gas composition, allowing the hole to be filled in part. This process is repeated to enable the welding to progress.[4] Because of such mechanism of penetration welding, it is necessary to keep filling the hole in order at the same time. Failing this, porosity occurs.

A-porosity observable in the welded parts of carbon steel and stainless steel occurs to the zone of beam of high energy density, which, mechanically is along the ripple line, cold shut or bonded parts and its internal surface is presumed to be subject to the vaporization element with high content of Mn. Also from the fact that the pattern of the internal surface is of cellular structure, the filling of hole of the molten metal in the vicinity of the drilled part of SM41 and SUS304N with large contents of O_2 and N_2 is scanty, but it is found in abundance in the upslope welding than in the downslope welding, it is considered the incidence of A-porosity is due to the incomplete filling by molten metal of the hole created by the drilling of the beam. This seems to be affected by the fluidity of the molten metal in the melting and solidification processes and the largeness of the

vaporization pressure of the composition element and gas composition like oxygen and nitrogen does not appear to have any direct influence.

As an example, we show the solubility curve[5), 6)] of nitrogen and hydrogen of Fe and Ni in **Fig. 3** and **4,** the nitrogen contained in SUS304N is below the melting point in the solid solution, and, on the top of that, it has a large content of Cr that increases the solid solubility of nitrogen.

If rapid condensation is further taken into consideration, the incidence of porosity by the discharge of gas is unthinkable, but further study about measurmeasurement of temperature is necessary since sudden drop of solubility of gas is conceivable in the neighborhood of boiling temperature.

As for R-porosity, it is closely related to spiking and it tends to occur, like A-porosity, along the ripple line and bonded parts. Its internal surface sees selective segregation of element of high vapor pressure as well as cellular structure, each material having a wide zone of incidence.

This led us to assume that the R-porosity incidence was due to the time lag of the inflow of molten metal to the hole formed by the extraordinarily quick cooling speed in the vicinity of the root part, and its effect is considered to be due to the unstability of the beam and the fluidity of the molten metal and the element of high vapor pressure.

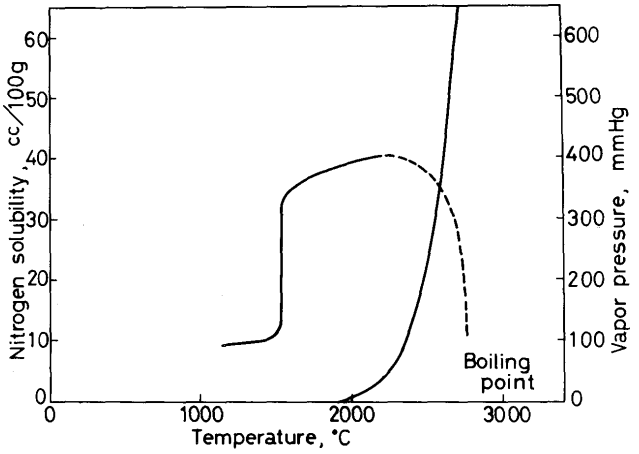

Fig. 3. Solubility curve of nitrogen and vapor pressure in iron.

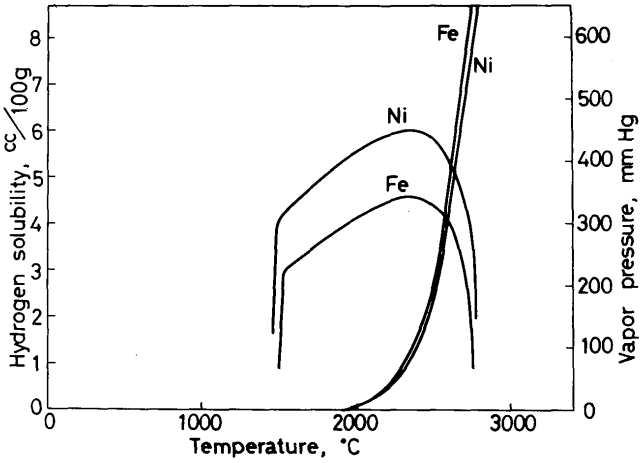

Fig. 4. Solubility curve of hydrogen and vapor pressure in iron. and nickel.

Meanwhile, the AR-porosity predominantly observable in aluminum alloys is noticeable in the zone of high energy density of the beam, and it is presumed to occur when the melting temperature is extremely high as compared with the melting point of the alloys. Vaporization of the metal of high vapor pressure or boiling is accompanied by the eruption of the molten metal with the result that discharge is liable to occur in the electron beam, even resulting in the welding failure.

This tendency is more prominent in 5083 and 7N01 with even higher vapor pressure element.
As to the prevention of the incidence of these porosities, it remains as a problem awaiting further study.

5. Conclusion

In order to determine the causes of formation of A-porosity, R-porosity and AR-porosity in weld metals, we studied weld-metallurgically the relativity between these porosities, materials and solidification structure in the electron beam welding of the carbon steel, austenitic stainless steel and aluminum alloys. Given below are the results obtained therefrom.

1) A-porosity observable in carbon steel and stainless steel occurs in the zone of high energy density of the beam, mostly along the ripple line, cold shut or bonded part. Its internal surface had the appearance of cellular structure with Mn segregation. The incidence of A-porosity appears to be due to the fact that the molten metal to be supplied to the hole formed by the drilling of the beam is not completely filled with molten metal, which is considered to have been caused by the vapor pressure of the vaporization element and the fluidity of the molten metal.
2) Gas was not present in the porosity observable in SM41 and SUS304N which contain oxygen and nitrogen in abundance. The oxygen and nitrogen in the weld metal indicated the same value as the base metal. In our opinion, the gas content to this extent has no direct bearing on the incidence of porosity.
3) R-porosity occurred over a wide area of a_b^* with crose relations with spiking, and mostly along the ripple line, same as A-porosity. The pattern of its internal surface had in most cases cellular structure, and abnormal segregation of high vapor pressure element in the alloys was recognized like

manganese in carbon steel and stainless steel, magnesium in 5083, and zinc in 7NO1.

4) AR-porosity observable in aluminum alloys was eminently present in the area of high energy density of the beam, mostly along the bonded part and its internal surface saw segregation of high vapor pressure element, same as R-porosity. AR-porosity incidence is caused by the evaporation of the metal of high vapor pressure or boiling, accompanied by the eruption of the weld metal with the result that discharge appears likely to occur in the electron beam.

References

1) Y. Arata, K. Terai, S. Matsuda: "Study on Characteristics of Weld Defect and Its Prevention in Electron Beam Welding (Report I)", Transactions of JWRI, Vol. 2, No. 1 (1973).
2) Y. Arata, I.Miyamoto: "Theoretical Analysis of Weld Penetration Due to High Energy Density Beam" Transactions of JWRI, Vol. 1, No. 1 (1972).
3) W. A. Tiller: "Solute Segregation During Ingot Solidification", Journal of JISI, August (1959).
4) Arata, et al: "Two-Three Studies of the Dynamic Behaviors of Welding Metal in the Electron Beam Welded Parts", Electron Beam Welding Study Material (1973).
5) Robert D. Pehlke, John F. Elliot: "Solubility of Nitrogen in Liquid Iron Alloys". Transactions of AIME, Vol. 218, Dec. (1960).
6) D. G. Howden, D. P. Milner: "Hydrogen Adsorption in Arc Welding", British Welding Journal, June (1963).